

PLANETARY DESERT AROUND COMPACT BINARIES: DYNAMICAL INSTABILITY TRIGGERED BY RESONANCE-INDUCED ECCENTRICITY EXCITATION

BIN LIU^{1,2}, DONG LAI^{3,4}

¹ Institute for Astronomy, School of Physics, Zhejiang University, Hangzhou 310027, China

² Center for Cosmology and Computational Astrophysics, Institute for Advanced Study in Physics, Zhejiang University, Hangzhou 310027, China

³ Tsung-Dao Lee Institute, Shanghai Jiao Tong University, Shanghai 200240, China

⁴ Department of Astronomy, Center for Astrophysics and Planetary Science, Cornell University, Ithaca, NY 14853, USA

Draft version March 3, 2026

ABSTRACT

Compact binaries with orbital periods shorter than about 7 days show an absence of transiting planets, a feature known as the “circumbinary planet desert”. The physical mechanism behind this desert remains unclear. We investigate its origin by simulating the long-term dynamics of multi-planet circumbinary systems with evolving inner binaries. Our simulations are based on the single-averaged secular equations that average only over the binary orbital period and fully incorporate planet-planet interactions. When an eccentric binary decays via tides, an outer planet can be captured into resonance advection in eccentricity, a state in which its apsidal precession locks with that of the binary, driving extreme eccentricity growth. While such growth can occur in a binary-single planet system, the parameter space is limited and may not necessarily induce instability. In a multi-planet system, however, the excited orbit inevitably crosses those of its neighbors, which triggers violent planet-planet scatterings and produces collisions or ejections. Crucially, these mutual gravitational interactions amplify the “localized” instability of a single planet into a system-wide chain reaction, drastically reshaping the orbital architecture and potentially clearing out the inner regions of planetary systems. Our results suggest that the resonance-induced instability provides a natural explanation for the observed circumbinary planet desert.

1. INTRODUCTION

Recent observations have identified over 30 planets (or candidates) orbiting stellar or brown-dwarf binaries through various detection methods, including planet transits (e.g., Doyle et al. 2011), timing variations of eclipsing binaries (e.g., Borkovits et al. 2016; Getley et al. 2017), radial velocity variations (e.g., Correia et al. 2005; Standing et al. 2023; Goldberg et al. 2023; Baycroft et al. 2025), microlensing (e.g., Bennett et al. 2016; Kuang et al. 2022; Han et al. 2024), and direct imaging (e.g., Burgasser et al. 2010; Kuzuhara et al. 2011; Delorme et al. 2013; Bryan et al. 2016; Bonavita et al. 2017; Dupuy et al. 2018, 2023; Janson et al. 2019, 2021). Among these, 14 transiting circumbinary planets (CBPs) have been discovered by the *Kepler* and *TESS* missions (e.g., Orosz et al. 2012a,b, 2019; Schwamb et al. 2013; Welsh et al. 2012, 2015; Kostov et al. 2020, 2021; Socia et al. 2020). These CBPs are in nearly coplanar orbits around their host binaries with periods $T_b \gtrsim 7$ days, and many reside near the dynamical stability limit (e.g., Armstrong et al. 2014; Windemuth et al. 2019). Such a configuration is consistent with planet’s formation history, in which the circumbinary protoplanetary disk is truncated by the binary’s torque, and the planets migrate inward until stalling near the disk inner edge (e.g., Nelson 2003; Kley & Nelson 2012; Kley & Haghighipour 2015; Rafikov & Silsbee 2014; Thun & Kley 2018; Penzlin et al. 2021).

However, a striking discrepancy emerges for compact binaries. Although eclipsing binaries with periods shorter than a few days are abundant in the *Kepler* target list, none have been found to host transiting planets (e.g., Orosz et al. 2012a). The absence of planets around compact binaries with $T_b \lesssim 7$ days is statistically significant and cannot be attributed to observational biases, as geometric transit probability favors detection around tighter systems. This deficit therefore points to a physical mechanism that either suppresses planet formation or destabilizes planetary orbits around the most compact stellar binaries.

Several mechanisms have been proposed. The tight binaries themselves may have formed through high-eccentricity migration driven by an inclined tertiary companion via the von Zeipel–Lidov–Kozai (ZLK) effect (e.g., von Zeipel 1910; Mazeh & Shaham 1979; Lidov 1962; Kozai 1962; Fabrycky & Tremaine 2007; Naoz & Fabrycky 2014; Moe & Kratter 2018), during which pre-existing CBPs are likely engulfed, ejected, or placed on distant, misaligned orbits (e.g., Martin et al. 2015; Muñoz & Lai 2015; Hamers et al. 2016). Other processes include evection resonances with external perturbers (e.g., Touma & Wisdom 1998; Xu & Lai 2016), or complex orbital evolution due to tidal synchronization and magnetic braking (e.g., Verbunt & Zwaan 1981; Ivanova & Taam 2003; Fleming et al. 2018). Alternatively, the observed “planetary desert” could partially

arise from observational concealment: surviving planets may become undetectable because of the reduced transit probability after the binary orbital shrinkage (e.g., Mogan & Zanazzi 2025).

In this work, we propose a dynamical mechanism that operates during the tidal decay of a stellar binary. Recent studies of coplanar triple systems show that when the inner binary undergoes orbital decay, a tertiary body can be captured into a state of resonance advection, where its apsidal precession locks with that of the binary, driving extreme eccentricity growth (e.g., Liu et al. 2015a; Liu & Lai 2020; Liu et al. 2022; Liu & Lai 2024; Farhat & Touma 2025). Based on this scenario, we study a system consisting of an eccentric stellar binary and multiple CBPs. As the binary experiences orbital shrinkage due to tidal dissipation, some of the planets are driven into apsidal precession resonances, exciting their eccentricities and triggering orbital crossings. The mutual gravitational interactions among the planets therefore become significant, driving widespread instabilities. We examine how this process reshapes the orbital architecture of the tidally evolved binary system.

This *Letter* is organized as follows. Section 2 reviews the physics of apsidal precession resonance capture and advection, and demonstrates how extreme eccentricity excitation can occur during the orbital shrinkage of inner binary. In Section 3, we show that the planet-planet scattering, triggered by the resonant eccentricity excitation, amplifies the “local” instability of a single planet into global system clearing through collisions and ejections. We summarize our conclusions in Section 4.

2. ECCENTRICITY EXCITATION DUE TO APSIDAL PRECESSION RESONANCE

We consider a hierarchical triple system in a coplanar configuration. The inner stellar binary consists of stars with masses m_1 and m_2 . The CBP with mass $m_p = 0.1M_J$ and radius $R_p = 0.2R_J$ ¹ orbits the center of mass of the inner binary. The semi-major axis and eccentricity of the stellar binary are denoted by a_b and e_b , and those of the planetary orbit by a_p and e_p , respectively. The orbital angular momenta are given by $\mathbf{L}_b \equiv \mathbf{L}_b \hat{\mathbf{L}}_b = \mu_b \sqrt{Gm_{12}a_b(1-e_b^2)} \hat{\mathbf{L}}_b$ and $\mathbf{L}_p \equiv \mathbf{L}_p \hat{\mathbf{L}}_p \simeq \mu_p \sqrt{Gm_{12}a_p(1-e_p^2)} \hat{\mathbf{L}}_p$, where $m_{12} \equiv m_1 + m_2$, $\mu_b \equiv m_1 m_2 / m_{12}$ and $\mu_p \simeq m_p$.

To study the long-term evolution of planetary orbits during the gradual tidal decay of the stellar binary, we adopt the single-averaged (SA; only averaging over the inner orbital period) secular equations of motion. The evolution of the inner binary itself is described by the

¹ Although CBPs primarily have radii between 0.3 and 0.8 R_J , their precise size distribution remains uncertain (e.g., Li et al. 2016; Welsh & Orosz 2018). We adopt a fiducial planetary radius of 0.2 R_J for our calculations. Note that larger radii would increase the probability of planet-planet collisions (see Section 3).

following vector equations:

$$\frac{d\mathbf{L}_b}{dt} = \frac{d\mathbf{L}_b}{dt} \Big|_{\text{TD}}, \quad (1)$$

$$\frac{d\mathbf{e}_b}{dt} = \frac{d\mathbf{e}_b}{dt} \Big|_{\text{GR}} + \frac{d\mathbf{e}_b}{dt} \Big|_{\text{TB}} + \frac{d\mathbf{e}_b}{dt} \Big|_{\text{TD}}, \quad (2)$$

where the subscripts denote contributions from general relativistic (GR) precession, precession due to the tidal bulge (TB), and tidal dissipation (TD), respectively. We adopt the formalism of Hut (1981); Leconte et al. (2010) and parameterize the rate of stellar tidal dissipation using a weak-friction model with a constant tidal lag time². The explicit forms of these terms can be found in Eggleton & Kiseleva-Eggleton (2001); Fabrycky & Tremaine (2007). Note that the evolution of the inner binary can also be affected by the tertiary companion through mechanisms such as the ZLK effect. However, because the CBP acts essentially as a test particle, its gravitational feedback on the binary can be safely neglected.

For the CBP’s orbit, the long-term evolution is governed by the perturbing potential induced by the inner stellar binary $\langle \Phi \rangle$:

$$\mu_p \frac{d^2 \mathbf{r}_p}{dt^2} = \nabla_{\mathbf{r}_p} \left(\frac{Gm_{12}m_p}{r_p} \right) - m_p \nabla_{\mathbf{r}_p} \langle \Phi \rangle, \quad (3)$$

where $\mathbf{r}_p \equiv r_p \hat{\mathbf{r}}_p$ denotes the position vector of the planet relative to the center of mass of the inner bodies. The averaged potential $\langle \Phi \rangle$ includes the quadrupole and octupole Newtonian gravitational potentials of the inner binary (e.g., Liu et al. 2015b; Liu & Lai 2018). Equations (1)-(3) fully determine the dynamics of the planetary orbit under the SA approximation.

We further consider systems with multiple planets. We develop a “Ring+Nbody” code and incorporate the mutual Newtonian gravitational potential between the planets into $\langle \Phi \rangle$ in Equation (3). Note that in the SA approximation, angular momentum is exchanged between the binary and the planets, but not energy. Between the planets, however, both energy and angular momentum exchange are allowed.

For a coplanar hierarchical triple, a secular eccentricity excitation can occur through apsidal precession resonance. This resonance operates when the precession rate of the inner binary periastron, $\dot{\omega}_b$, matches that of the outer (planetary) orbit, $\dot{\omega}_p$ (e.g., Liu et al. 2015a; Liu & Lai 2020; Liu et al. 2022):

$$\dot{\omega}_b \simeq \dot{\omega}_p. \quad (4)$$

When this condition is satisfied, efficient eccentricity exchange between the two orbits becomes possible.

² In this framework, the viscous dissipation timescale t_V is the primary source of uncertainty. Although t_V varies by 1–2 orders of magnitude across stellar types, we adopt $t_V = 1\text{yr}$ as our fiducial value. Tidal dissipation is included for only m_1 and assume the rotation rate is pseudo-synchronous. The effective tidal quality factor is $Q = 4kGm_1 t_V / [3(1+2k)^2 R_1^3 n_b]$ with $k = 0.014$, where $n_b = (Gm_{12}/a_b^3)^{1/2}$ is the mean motion of the inner binary.

For our system, the inner binary’s precession rate is dominated by general relativistic (1PN) pericenter advance and the non-dissipative tidal bulge contribution

$$\dot{\omega}_b = \dot{\omega}_{\text{GR}} + \dot{\omega}_{\text{TB}}, \quad (5)$$

where

$$\dot{\omega}_{\text{GR}} = \frac{3G^{3/2}m_{12}^{3/2}}{c^2a_b^{5/2}(1-e_b^2)}, \quad (6)$$

and the tidal bulge contribution (for m_1) takes the form (e.g., Liu et al. 2015b)

$$\dot{\omega}_{\text{TB}} = \frac{15}{8} \sqrt{\frac{Gm_{12}}{a_b^3}} \left(\frac{m_2}{m_1}\right) \left(\frac{R_1}{a_b}\right)^5 k \frac{8 + 12e_b^2 + e_b^4}{(1-e_b^2)^5}, \quad (7)$$

where $k = 0.014$ and $R_1 \simeq 0.85m_1^{0.67}R_\odot$ are the classical apsidal motion constant and the radius of m_1 , respectively (e.g., Demircan & Kahraman 1991). For simplicity, we neglect the precession induced by the rotational bulge - this is of similar order as $\dot{\omega}_{\text{TB}}$ for pseudo-synchronous rotation.

The planetary orbit precession rate arises from the secular gravitational perturbation of the binary in quadrupole order (e.g., Liu et al. 2015b)

$$\dot{\omega}_p = \frac{3}{4} \left(\frac{G\mu_b m_p a_b^2}{a_p^3}\right) \frac{1}{L_p(1-e_p^2)^{3/2}}. \quad (8)$$

Recent studies have shown that if the inner binary undergoes adiabatic orbital decay (e.g., via GW emission or tidal dissipation), the tertiary can experience extreme eccentricity excitation (e.g., Liu & Lai 2024; Farhat & Touma 2025). In particular, it can be captured into a state of resonance advection, during which the two precession rates are in a 1 : 1 commensurability until the binary circularization is reached. This resonance-locking phenomenon leads to a continuous growth of the outer orbit eccentricity e_p .

Three principal criteria must be satisfied for successful resonance capture and advection (Liu & Lai 2024): *i*) Adiabatic evolution: The timescale of binary orbital decay must be much longer than the characteristic secular timescale $|\dot{a}_b/a_b|^{-1} \gg |\dot{\omega}_p|^{-1}$. *ii*) Direction of resonance crossing: The system must encounter the resonance from the regime $\dot{\omega}_p > \dot{\omega}_b$ towards $\dot{\omega}_p < \dot{\omega}_b$. *iii*) Small initial outer binary eccentricity: The initial $e_{p,0}$ must be less than about $15(m_1 - m_2)a_b e_b(4 + 3e_b^2)/(8m_{12}a_p)$ at the moment of $\dot{\omega}_b \simeq \dot{\omega}_p$.

To illustrate the resonance advection, Figure 1 depicts the long-term evolution of the CBP during the orbital decay of the stellar binary due to tidal dissipation. We consider four planets with different initial separations, and each is initially placed outside the critical stable semi-major axis $a_{p,c}$ given by the empirical formula of Holman & Wiegert (1999):

$$a_{p,c} = a_b(1.6 + 5.1e_b - 2.22e_b^2 + 4.12\mu_c - 4.27e_b\mu_c - 5.09\mu_c^2 + 4.61e_b^2\mu_c^2), \quad (9)$$

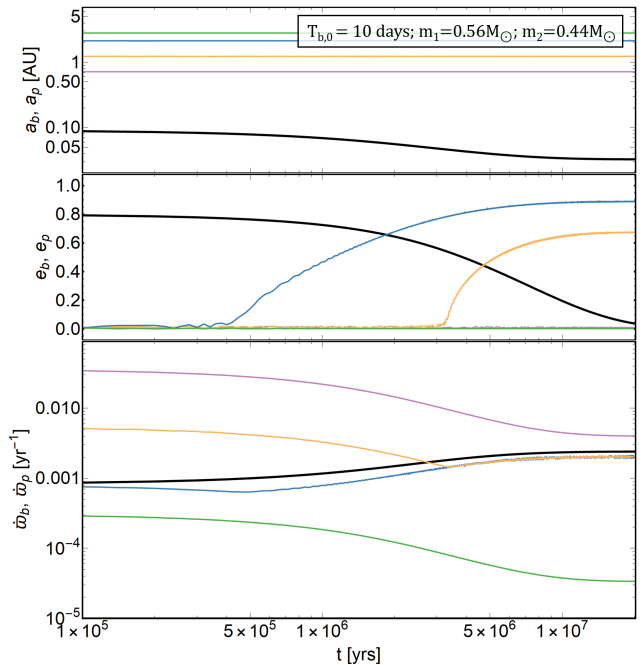


FIG. 1.— Evolution of a stellar binary (black) with four (non-interacting) circumbinary planets in a coplanar configuration. The masses of the inner stellar binary are $m_1 = 0.56M_\odot$ and $m_2 = 0.46M_\odot$. The initial semimajor axis and eccentricity of the inner binary are $a_{b,0} = 0.09\text{AU}$ and $e_{b,0} = 0.8$. The outer orbits, ordered by increasing distance, have initial semimajor axes $a_p = 0.72\text{AU}$, 1.24AU , 2.13AU and 2.81AU . All four begin with eccentricity $e_{p,0} = 0.001$. The longitudes of pericenter for both the binary and the planetary orbits are initialized to $\varpi_{b,0} = \varpi_{p,0} = 0$. Each binary–planet system is evolved independently (i.e., without planet–planet interactions) by integrating the single-averaged (SA) secular equations (Equations 1-3), where the tidal dissipation is included in the binary evolution (top and middle panels). The bottom panel shows the corresponding apsidal precession rates computed from Equations (5) and (8).

where $\mu_c = m_2/m_{12}$. The results are obtained by integrating the SA secular equations for individual triples, i.e., the planet–planet interactions are not included.

Driven by tidal dissipation, we see that the binary semi-major axis a_b shrinks while its eccentricity e_b decreases, reaching a final separation of $a_{b,f} \simeq 0.03\text{AU}$ (corresponding to an orbital period of 2.2 days). The inner binary apsidal precession rate $\dot{\omega}_b$ (Equation 5) increases monotonically, whereas the planetary orbital precession rate $\dot{\omega}_p$ (Equation 8) decreases as the binary’s gravitational potential weakens. The evolution leads to three distinct outcomes. For initially distant planets ($a_p = 2.81\text{AU}$), the initial precession rate $\dot{\omega}_{p,0}$ is smaller than $\dot{\omega}_{b,0}$; hence the precession matching condition is never satisfied and no resonance excitation occurs. When the planet is closer ($a_p = 2.13\text{AU}$ and $a_p = 1.24\text{AU}$), the initial configuration satisfies $\dot{\omega}_{b,0} \lesssim \dot{\omega}_{p,0}$. As $\dot{\omega}_b$ grows and overtakes $\dot{\omega}_p$, the system is captured into resonance advection. The two precession rates then evolve in lockstep until the inner binary is circularized, driving a continuous rise in the planetary eccentricity e_p . A comparison between the planetary pericenter distance and the critical semi-major axis $a_{p,c}$ (Equation 9) shows

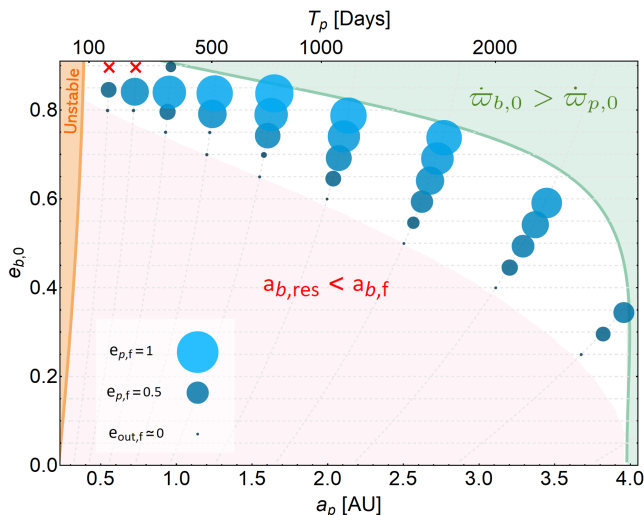


FIG. 2.— Parameter space in the $a_p - e_{b,0}$ plane showing the regime for resonance capture and advection during the orbital decay of the stellar binary. The orbital period T_p for planets at different distances is labeled at the top. We choose the same stellar binary as in Figure 1, varying only the initial binary eccentricity $e_{b,0}$. The orange region marks systems that are dynamically unstable according to Equation (9) by considering initially circular planetary orbits. The initial orbits of the planets are spaced according to the mutual Hill instability criterion with $K_c = 10$ in Equation (10). The green region corresponds to systems in which the initial apsidal precession rate of the inner binary exceeds the precession rate of the planetary orbit. The pink region represents systems for which the binary semimajor axis never shrinks to the value required to trigger apsidal precession resonance before tidal decay ceases. Systems in the green and pink regions would not experience resonance during the binary orbital decay. For each planetary orbit, we integrate the single-averaged (SA) secular equations until tidal evolution ends and record the final eccentricity $e_{p,f}$, whose value is represented by the size of the circles. The red crosses indicate orbits that become unbound in the numerical integration—either the semimajor axis turns negative or the eccentricity exceeds unity.

that no CPB becomes unstable during this phase. For the innermost planet ($a_p = 0.72$ AU), $\dot{\omega}_p$ remains larger than $\dot{\omega}_b$ throughout the evolution, and no resonance passage occurs. We therefore find that resonant eccentricity excitation requires that the binary semi-major axis at resonance, $a_{b,\text{res}}$ (obtained by solving Equation 4 for a_b) exceed its final value $a_{b,f}$ when tidal evolution ceases. Note that this is different from the system that undergoes orbital decay due to gravitational wave emission or magnetic braking (see Liu & Lai 2024). In those cases, $\dot{\omega}_b$ continues to increase, allowing the tertiary to eventually satisfy the resonance condition.

To characterize the parameter dependence of the resonance excitation, Figure 2 maps the parameter space in the $a_p - e_{b,0}$ plane where the eccentricity of a planetary orbit e_p can be excited. For a given binary, the initial orbital spacing of the planets follows the Hill instability criterion

$$a_{p,j} - a_{p,i} = K_c \left(\frac{a_{p,i} + a_{p,j}}{2} \right) \left(\frac{2m_p}{m_{12}} \right)^{1/3}, \quad (10)$$

where i, j denote adjacent planets, and K_c is a constant. We adopt $K_c = 10$ in this study (e.g., Pu & Lai 2021)

and set the innermost planet’s semi-major axis to $1.5 a_{p,c}$ (see Equation 9).

Figure 2 reveals a finite range of planetary semi-major axes that permits e_p -excitation. A planet cannot be captured into apsidal precession resonance during binary orbital decay in the green and pink regions. First, if the planet is too close to the binary, the resonance location $a_{b,\text{res}}$ falls inside the binary’s final orbital radius $a_{b,f}$ (see the evolution of the $a_p = 0.72$ AU orbit in Figure 1). Second, if the planet is too distant, the initial precession rates satisfy $\dot{\omega}_{b,0} > \dot{\omega}_{p,0}$ (see the evolution of the $a_p = 2.81$ AU orbit in Figure 1). The parameter space for systems capable of undergoing resonance advection is limited, and becomes narrow as the initial binary eccentricity $e_{b,0}$ decreases. This results from the competition between the tidal decay timescale and the eccentricity growth timescale. Moreover, for a given $e_{b,0}$, planets located at larger a_p can achieve higher final eccentricities. This results from their prolonged resonance locking phase, which persists over most of the binary tidal decay, as illustrated in Figure 1.

3. SECULAR EVOLUTION AND GRAVITATIONAL SCATTERING IN MULTI-PLANET SYSTEMS

We now consider systems with multiple planets that are interacting with each other. Once a planet’s eccentricity e_p undergoes resonant excitation, the periastron distance of the orbit decreases sharply while the apastron distance expands. This causes the planetary orbit to cross those of its neighbors, triggering close encounters and gravitational scattering. At this stage, mutual gravitational interactions among planets replace the long-term resonant perturbations from the host binary as the dominant driver of the system dynamics. This scattering process redistributes both angular momentum and orbital energy, resulting in drastic changes to the planetary semi-major axes, and potentially leading to either ejection of the planets or collisions with neighboring bodies.

3.1. Case study: two circumbinary planets

When two planets undergo orbital crossing and enter the regime of strong scattering, their evolutionary outcomes include three types:

i) Ejection. Previous N-body numerical experiments indicate that in systems comprising two planets on initially unstable orbits, the averaged timescale for an ejection can be approximated as

$$T_{\text{ej}} \simeq 0.06^2 \left(\frac{m_{12}}{m_{p,i}} \right)^2 \left(1 + \frac{m_{p,j}}{m_{p,i}} \right)^4 T_{p,j}, \quad (11)$$

where $T_{p,j}$ is the initial orbital period of $m_{p,j}$ (e.g., Pu & Lai 2021; Li et al. 2022). Equation (11) implies that ejection typically requires many orbital periods. In our simulations, an ejection event is recorded if the semi-major axis of a planet becomes negative ($a_p < 0$) or if its eccentricity exceeds unity ($e_p > 1$).

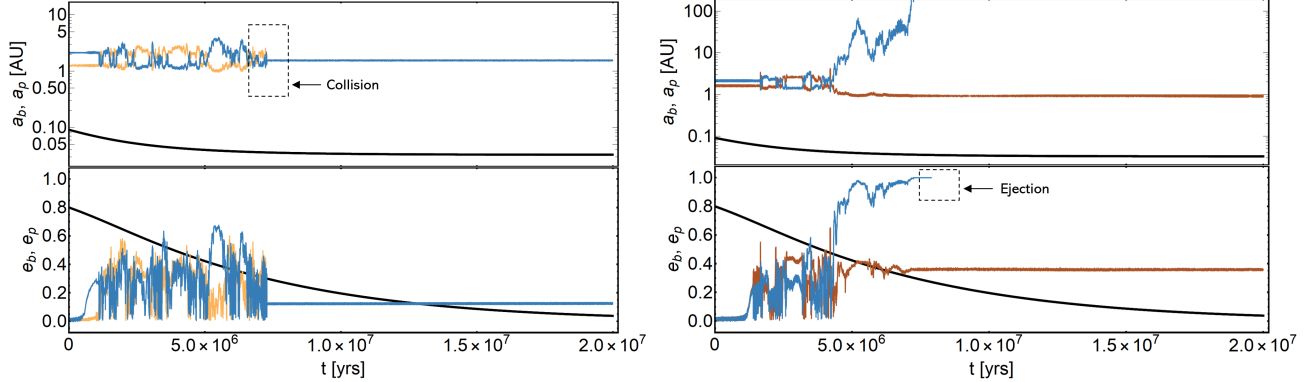


FIG. 3.— Similar to Figure 1, but including mutual gravitational interaction between two CBPs. The initial longitude of pericenter of each planet is randomly chosen between 0 and 2π . The evolution of the system can lead to either collision or ejection. Left panel: Two planets with initial semimajor axes $a_p = 2.13\text{AU}$ and 1.24AU collide into a single body. Right panel: One planet initially located at $a_p = 2.13\text{AU}$ is ejected from the system.

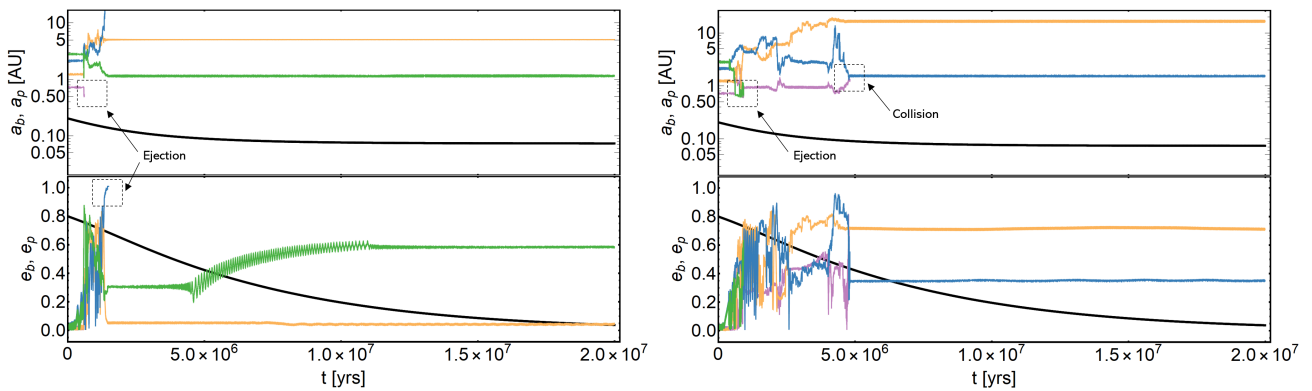


FIG. 4.— Same system as in Figure 1, but with mutual gravitational interactions among all four planets. The initial longitude of pericenter of each CBP’s orbit is randomly chosen in the range $[0 - 2\pi]$. The eccentricity of the planetary orbit grows significantly, even for the planet that does not undergo resonant eccentricity-excitation in isolation. The resulting orbital crossings trigger strong interactions between planets, which reshape the orbital architecture and lead to either an ejection event (left panel) or a collision event (right panel).

ii) Collision. Whether two planets collide or scatter apart depends primarily on the “Safronov number”:

$$\Theta \equiv \left(\frac{v_{\text{esc}}}{v_{\text{orb}}} \right)^2, \quad (12)$$

where v_{esc} is the escape velocity of the planet and v_{orb} is its orbital velocity around the star. If the Safronov number is less than unity, a significant fraction of planetary collisions are expected. In our simulations, a collision is identified when the separation between two planets becomes smaller than the sum of their radii, $2R_p$. Such an event is denoted as, for example, Orbit i –Orbit j ($O_i - O_j$ hereafter). After a collision, we continue to track the evolution of the collision remnant, which has a mass equal to the sum of the colliding bodies but an unchanged radius, and is labeled as O_j' . The position and velocity of this remnant are set by momentum conservation at the instant of collision.

iii) Tidal disruption. The third possible outcome involves interactions between a planet and an individual star of the host binary, such as tidal disruption. However, because the SA equations can not resolve the precise positions of the stars along their orbits, such a process is not considered in this study.

We explore the evolution of a two-planet system, as shown in Figure 3. The initial semi-major axes of both planets lie within the parameter space for resonant excitation identified in Figure 2. As the host binary shrinks, the eccentricities of the two planets are sequentially excited. Orbital crossing between their elongated orbits occur, triggering strong scattering. The left panel illustrates a case where the two planets collide and merge into one body. The right panel illustrates an outcome in which one planet is ejected from the system.

3.2. Case study: four circumbinary planets

Figure 4 shows the evolution of a system containing four interacting planets, with the initial parameters of the system identical to those in Figure 1.

A key finding is that planet-planet interactions can dramatically extend the parameter space for eccentricity excitation. Even planets that would remain stable in isolation (e.g., those located at $a_p = 0.72\text{AU}$ or 2.81AU , shown in Figures 1-2) are perturbed by neighboring planets whose eccentricities are resonantly excited. These perturbations induce substantial indirect eccentricity growth, leading to orbital crossings that allow the planets to approach closely to each other and

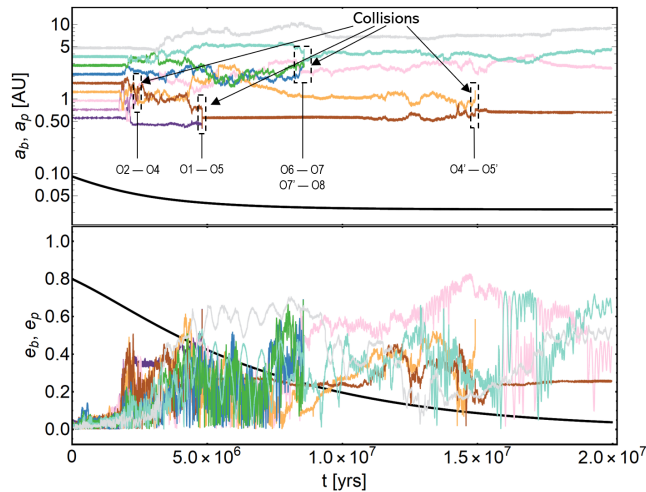


FIG. 5.— The evolution of 9-planet system during tidal decay of the host binary, with mutual planet-planet gravitational interactions included. The system parameters are taken from Figure 2, with $e_{b,0} = 0.8$ as a fiducial value: The planets are ordered by increasing distance with semimajor axes $a_p = 0.55\text{AU}, 0.72\text{AU}, 0.94\text{AU}, 1.24\text{AU}, 1.63\text{AU}, 2.13\text{AU}, 2.81\text{AU}, 3.69\text{AU}, 4.85\text{AU}$. Mutual interactions lead to frequent planetary collisions, with some planets experiencing repeated collisions, e.g., O2 and O4 merge into O4', O1 and O5 merge into O5', and then O4' and O5' collide to form O5''.

produce mutual collisions or ejections. We see that the evolution of the planets is strongly chaotic, evidenced by the sensitive dependence of the outcomes (left vs. right panels) on the initial conditions.

3.3. Case study: nine circumbinary planets

To evaluate how a “localized” instability triggered by resonance propagates throughout the planetary system via gravitational coupling among the planets, we simulate a system with nine planets and carry out Monte Carlo simulations with random initial longitude of pericenter to obtain statistical results.

In Figure 5, the nine planets are initially spaced according to Equation (10) with $K_c = 10$. During the tidal decay of the binary, only a subset of planets, concentrated in the region $0.9\text{AU} \lesssim a_p \lesssim 2.2\text{AU}$, are directly excited by the apsidal precession resonance. We see that the orbital evolution becomes increasingly complex as the number of planets increases. Nevertheless, the scattering events induced by mutual gravitational interactions quickly spread throughout the inner planetary system.

For the planetary systems of interest here, located within a few AU of the host binary, the orbital velocity typically exceeds the escape velocity of the planet. Consequently, $\Theta \lesssim 1$ (Equation 12), indicating that a substantial fraction of planetary encounters are expected to result in collisions. Based on the result in Figure 6, on average, each simulation produces $\sim 3-4$ collision events. The violent dynamical process significantly reshapes the orbital architecture of the system, manifesting in two features: *i*) the survival rate of planets in the inner region is extremely low, with the innermost surviving bodies typically being the products of mergers; *ii*) planets in

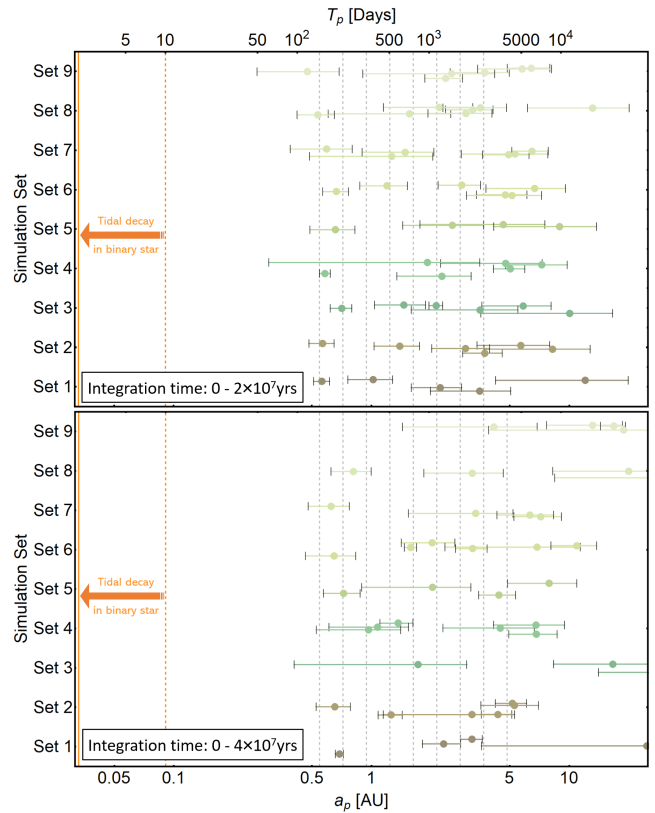


FIG. 6.— Architecture of planetary orbits after the tidal evolution of the host binary has ceased. The results are based on statistical outcomes from 9 runs of the system depicted in Figure 5, each with a random initial value of the longitude of pericenter $\varpi_{p,0}$. Note that the results in Figure 5 correspond to “Set 5” here. For each set of numerical integration, the color-coded circles denote the semi-major axes (or orbital periods in days) of the survived planets. The horizontal line associated with each circle spans the corresponding periastron and apastron distances, indicating the orbital extent due to nonzero eccentricity. The gray vertical dashed line marks the initial semi-major axes of the nine planets. The orange vertical dashed line indicates the initial semi-major axis of the stellar binary $a_{b,0}$, while the orange vertical solid line shows the binary separation after it has circularized. The results in the upper and lower panels correspond to different integration time, as labeled.

the outer region exhibit a higher survival rate, but their orbits generally migrate outward and retain substantial eccentricities.

It is important to emphasize that even after the stellar binary orbit has circularized, many planetary orbits retain high eccentricities and continue to cross one another, as shown in the upper panel of Figure 6. This implies that the surviving orbits remain “unstable”, and their erratic evolution will continue. Thereby, these planets, which have undergone large-amplitude variation of e_p , are likely to be either ejected from the system or to collide with other CBPs or the central binary stars, leaving only a very small number of survivors in the inner region (as illustrated by the example in the lower panel of Figure 6).

4. CONCLUSION AND DISCUSSION

We have studied the evolution and survival of planets around stellar binaries that undergo orbital decay via the tidal dissipation. An eccentric binary experiencing tidal decay can excite the orbital eccentricities of surrounding planets through apsidal precession resonance. Once a planet acquires substantial eccentricity, its elongated orbit crosses those of neighboring planets, triggering planet-planet scatterings. This process initiates a “chain reaction”, which greatly destabilize the orbits of planets that do not experience eccentricity excitation directly, leading to planet collision or ejection. By performing a series of numerical integrations, we show that the mutual gravitational interactions in multi-planet systems play a major role in amplifying a localized instability due to resonant eccentricity-excitation into a system-wide catastrophe. Our results suggest that this dynamical process can clear out the inner regions of planetary systems around binaries, thereby helping to explain the observed “planetary desert” around compact binaries with orbital period less than ~ 7 days.

Throughout this *Letter*, we have adopted a representative set of parameters to illustrate the dynamical process. While our numerical examples assume a fiducial binary initial eccentricity of $e_{b,0} = 0.8$, the resonance-induced instability can occur for systems with $e_{b,0} \gtrsim 0.5$. A lower initial binary eccentricity would restrict the range of planetary orbits susceptible to eccentricity excitation

and prolong the timescale of stellar tidal decay. In general, once a planet acquires significant eccentricity excitation, planet-planet interactions would spread the instability to a wide region of the system. In our study, we have considered a fiducial binary configuration and assumed uniform planetary masses. These choices set the characteristic timescale for eccentricity excitation. Varying the planetary mass distribution would also modify the Hill radii and scattering cross sections, which in turn could change the efficiency of dynamical clearing. A systematic exploration across a broader parameter space lies beyond the scope of the present study and is reserved for future work.

To fully explain the observational statistics of circumbinary planets, future population synthesis simulations that couple binary tidal evolution and the dynamical processes identified here is essential. Such simulations will enable quantitative predictions of planet occurrence rates around binaries of different periods.

5. ACKNOWLEDGMENTS

B. L. thanks Yanqin Wu and Douglas N.C.Lin for useful discussions. B. L. acknowledges support from the National Natural Science Foundation of China (Grant No. 12433008) and National Key Research and Development Program of China (No. 2023YFB3002502).

REFERENCES

- Armstrong, D. J., Osborn, H. P., Brown, D. J. A., et al. 2014, *MNRAS*, **444**, 1873
 Bate, M. R. 2009, *MNRAS*, **392**, 590
 Bate, M. R. 2019, *MNRAS*, **484**, 2341
 Baycroft, T. A., Santerne, A., Triaud, A. H. M. J., et al. 2025, *MNRAS*, **541**, 2801
 Bennett, D. P., Rhie, S. H., Udalski, A., et al. 2016, *AJ*, **152**, 125
 Bonavita, M., D’Orazi, V., Mesa, D., et al. 2017, *A&A*, **608**, A106
 Borkovits, T., Hajdu, T., Sztakovics, J., et al. 2016, *MNRAS*, **455**, 4136
 Bryan, M. L., Bowler, B. P., Knutson, H. A., et al. 2016, *ApJ*, **827**, 100
 Burgasser, A. J., Simcoe, R. A., Bochanski, J. J., et al. 2010, *ApJ*, **725**, 1405
 Correia, A. C. M., Udry, S., Mayor, M., et al. 2005, *A&A*, **440**, 751
 Delorme, P., Gagné, J., Girard, J. H., et al. 2013, *A&A*, **553**, L5
 Demircan, O., & Kahraman, G. 1991, *Ap&SS*, **181**, 313
 Doyle, L. R., Carter, J. A., Fabrycky, D. C., et al. 2011, *Science*, **333**, 1602
 Dupuy, T. J., Liu, M. C., Allers, K. N., et al. 2018, *AJ*, **156**, 57
 Dupuy, T. J., Liu, M. C., Evans, E. L., et al. 2023, *MNRAS*, **519**, 1688
 Eggleton, P. P., & Kiseleva-Eggleton, L. 2001, *ApJ*, **562**, 1012
 Fabrycky, D., & Tremaine, S. 2007, *ApJ*, **669**, 1298
 Farhat, M., & Touma, J. 2025, *ApJL*, **995**, L23
 Fleming, D. P., Barnes, R., Graham, D. E., et al. 2018, *ApJ*, **858**, 86
 Getley, A. K., Carter, B., King, R., & O’Toole, S. 2017, *MNRAS*, **468**, 2932
 Goldberg, M., Fabrycky, D., Martin, D. V., et al. 2023, *MNRAS*, **525**, 4628
 Goldreich, P., & Tremaine, S. 1980, *ApJ*, **241**, 425
 Hamers, A. S., Perets, H. B., & Portegies Zwart, S. F. 2016, *MNRAS*, **455**, 3180
 Han, C., Udalski, A., Jung, Y. K., et al. 2024, *A&A*, **685**, A16
 Holman, M. J., & Wiegert, P. A. 1999, *AJ*, **117**, 621
 Hut, P. 1981, *A&A*, **99**, 126
 Ivanova, N., & Taam, R. E. 2003, *ApJ*, **599**, 516
 Janson, M., Asensio-Torres, R., André, D., et al. 2019, *A&A*, **626**, A99
 Janson, M., Gratton, R., Rodet, L., et al. 2021, *Natur*, **600**, 231
 Kley, W., & Haghighipour, N. 2015, *A&A*, **581**, A20
 Kley, W., & Nelson, R. P. 2012, *ARA&A*, **50**, 211
 Kostov, V. B., Orosz, J. A., Feinstein, A. D., et al. 2020, *AJ*, **159**, 253
 Kostov, V. B., Powell, B. P., Orosz, J. A., et al. 2021, *AJ*, **162**, 234
 Kozai, Y. 1962, *AJ*, **67**, 591
 Kuang, R., Zang, W., Jung, Y. K., et al. 2022, *MNRAS*, **516**, 1704
 Kuzuhara, M., Tamura, M., Ishii, M., et al. 2011, *AJ*, **141**, 119
 Lecote, J., Chabrier, G., Baraffe, I., et al. 2010, *A&A*, **516**, A64
 Li, G., Holman, M. J., & Tao, M. 2016, *ApJ*, **831**, 96
 Li, J., Lai, D., & Rodet, L. 2022, *ApJ*, **934**, 154
 Lidov, M. L. 1962, *P&SS*, **9**, 719
 Liu, B., Lai, D., & Yuan, Y.-F. 2015a, *PhRvD*, **92**, 124048
 Liu, B., Muñoz, D. J., & Lai, D. 2015b, *MNRAS*, **447**, 747
 Liu, B., & Lai, D. 2018, *ApJ*, **863**, 68
 Liu, B., & Lai, D. 2020, *PhRvD*, **102**, 023020
 Liu, B., D’Orazio, D. J., Vigna-Gómez, A., et al. 2022, *PhRvD*, **106**, 123010
 Liu, B., & Lai, D. 2024, *PhRvL*, **132**, 231403
 Martin, D. V., Mazeh, T., & Fabrycky, D. C. 2015, *MNRAS*, **453**, 3554
 Mazeh, T., & Shaham, J. 1979, *A&A*, **77**, 145
 Moe, M., & Kratter, K. M. 2018, *ApJ*, **854**, 44
 Mogan, S., & Zanazzi, J. J. 2025, *ApJ*, **988**, 150
 Muñoz, D. J., & Lai, D. 2015, *PNAS*, **112**, 9264
 Naoz, S., & Fabrycky, D. C. 2014, *ApJ*, **793**, 137
 Nelson, R. P. 2003, *MNRAS*, **345**, 233
 Orosz, J. A., Welsh, W. F., Carter, J. A., et al. 2012a, *Science*, **337**, 1511
 Orosz, J. A., Welsh, W. F., Carter, J. A., et al. 2012b, *ApJ*, **758**, 87
 Orosz, J. A., Welsh, W. F., Haghighipour, N., et al. 2019, *AJ*, **157**, 174
 Penzlin, A. B., Kley, W., & Nelson, R. P. 2021, *A&A*, **645**, A68
 Pu, B., & Lai, D. 2021, *MNRAS*, **508**, 597
 Rafikov, R. R., & Silsbee, K. 2014, *ApJ*, **798**, 69
 Schwamb, M. E., Orosz, J. A., Carter, J. A., et al. 2013, *ApJ*, **768**, 127
 Socia, Q. J., Welsh, W. F., Orosz, J. A., et al. 2020, *AJ*, **159**, 94
 Standing, M. R., Sairam, L., Martin, D. V., et al. 2023, *NatAs*, **7**, 702
 Thun, D., & Kley, W. 2018, *A&A*, **616**, A47

- Tokovinin, A., & Moe, M. 2020, MNRAS, **491**, 5158
Touma, J., & Wisdom, J. 1998, AJ, **115**, 1653
Verbunt, F., & Zwaan, C. 1981, A&A, **100**, L7
von Zeipel, H. 1910, AN, **183**, 345
Welsh, W. F., Orosz, J. A., Carter, J. A., et al. 2012, Natur, **481**, 475
Welsh, W. F., Orosz, J. A., Short, D. R., et al. 2015, ApJ, **809**, 26
Welsh, W. F., & Orosz, J. A. 2018, in Handbook of Exoplanets, ed. H. J. Deeg & J. A. Belmonte (Cham: Springer), 34
Windemuth, D., Agol, E., Ali, A., et al. 2019, MNRAS, **489**, 1644
Xu, W., & Lai, D. 2016, MNRAS, **459**, 2925